Journal of Power Sources 251 (2014) 338–343

Contents lists available at ScienceDirect

Journal of Power Sources

journal homepage: www.elsevier.com/locate/jpowsour

Short communication

Microwave-assisted synthesis of hybrid $Co_xNi_{1-x}(OH)_2$ nanosheets: Tuning the composition for high performance supercapacitor

Gen Chen [a], Steven S. Liaw [a], Binsong Li [b], Yun Xu [a], Marco Dunwell [a], Shuguang Deng [a], Hongyou Fan [b], Hongmei Luo [a,*]

[a] Department of Chemical Engineering, New Mexico State University, Las Cruces, NM 88003, United States
[b] Advanced Materials Laboratory, Sandia National Laboratories, Albuquerque, NM 87106, United States

HIGHLIGHTS

- Hybrid $Co_xNi_{1-x}(OH)_2$ nanosheets can be prepared *via* a facile microwave-assisted route.
- The Co:Ni ratio depended size and crystal structure were demonstrated.
- The Co:Ni ratio depended electrochemical performance was proved.
- $Co_{0.2}Ni_{0.8}(OH)_2$ hexagonal nanosheets deliver a high specific capacitance of 1170 F g^{-1} at a current density of 4 A g^{-1}.

GRAPHICAL ABSTRACT

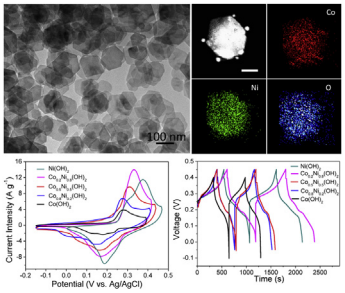

ARTICLE INFO

Article history:
Received 19 September 2013
Received in revised form
9 November 2013
Accepted 19 November 2013
Available online 4 December 2013

Keywords:
Microwave-assisted
Hybrid hydroxides
Nanosheet
Electrochemical
Supercapacitors

ABSTRACT

Hybrid $Co_xNi_{1-x}(OH)_2$ nanosheets have been successfully synthesized *via* a facile microwave-assisted synthetic route. The size of $Co_xNi_{1-x}(OH)_2$ nanosheets decreases with the increase of nickel amount; however, the layered crystal structure can be maintained at any ratios of Co:Ni due to the chemical and physical similarities between these two elements. The lattice spacing of the hexagonal nanosheets can be slightly varied by adjusting the ratios of Co:Ni. The hybrid $Co_{0.2}Ni_{0.8}(OH)_2$ hexagonal nanosheets deliver a high capacity of above 1170 F g^{-1} at a current density of 4 A g^{-1}. The higher specific capacitance of $Co_{0.2}Ni_{0.8}(OH)_2$ nanosheets than their monometallic counterpart could be attributed to the enhancement of the electro-active sites participated in the redox reaction due to the possible valence interchange or charge hopping between Co and Ni cations. These results indicate the importance of layered hydroxide nanosheets with tuned transition-metal composition for high-performance energy storage devices.

1. Introduction

Many important and challenging research areas have the potential to significantly affect our future energy needs. For example, energy efficiency, the integration of energy sources with electricity transmission, and energy storage are of vital significance, but it remains a sophisticated challenge to improve the energy transfer efficiency [1–3]. Electrochemical capacitors (ECs), also known as pseudocapacitors or supercapacitors (SCs), have received great attention for potential applications in electric vehicles and hybrid electric vehicles because of their ability to store energy, meanwhile with the advantage of delivering the stored energy much more rapidly than batteries, namely power density [4–6]. However, to become primary devices for power supply, supercapacitors must be developed further to improve their abilities to deliver high energy and power simultaneously. In this concern, many efforts have been

* Corresponding author. Tel.: +1 575 646 4204; fax: +1 575 646 7706.
E-mail address: hluo@nmsu.edu (H. Luo).

0378-7753/$ – see front matter © 2013 Elsevier B.V. All rights reserved.
http://dx.doi.org/10.1016/j.jpowsour.2013.11.070

devoted to the investigation of pseudocapacitive transition-metal-based oxides or hydroxides, such as MnO_2 [7,8], NiO [9], Co_3O_4 [10,11], $Co(OH)_2$ [12,13], $Ni(OH)_2$ [14], and mixed metal oxides such as $NiCo_2O_4$ [15–17], because they can produce much higher specific capacitances than typical carbon-based electric double-layer capacitors and electronically conducting polymers.

Among these composite materials, Co–Ni hydroxides have drawn increasing attention because the introduction of cobalt can not only reduce the resistance of the electrode and raise the oxygen overpotential, but also participate in the electrochemical redox reaction [18,19]. Particularly, layered transition-metal hydroxides with large interlayer spacing display desirable electrochemical activity derived from their redox nature and better accessibility for the reaction species [20]. The similarities between Ni and Co offer opportunities to yield hybrid materials by the widely applied technological doping strategy. If Ni and Co are co-incorporated in the host layer, an improved capacity and cycling stability may be expected in comparison with monometallic hydroxides, which therefore offer an effective way to achieve high electrochemical performance.

Various synthetic approaches have been adopted or improved for preparing $Co(OH)_2$ and $Ni(OH)_2$ nanomaterials, such as sonochemical [21], solvothermal [22,23], and hydrothermal process [24,25]. Among these strategies, the microwave-assisted route is a fast, simple, and effective method for synthesis of transition metal hydroxides due to its clean, cheap, and efficient heating [26–28]. Here we describe a facile and reliable microwave-assisted route for the production of high-quality Co–Ni hydroxide nanosheets with a tunable composition. The total reaction duration was only 3 min. The hybrid Co–Ni hydroxides possess almost unchanged crystal structural feature. Significantly, electrochemical characterizations reveal that bimetallic Co–Ni hydroxide nanosheets exhibit a high specific capacitance and excellent cycling stability, which may enable their practical applications as active electrode materials in energy storage devices.

2. Experimental

2.1. Synthesis of Co–Ni hydroxide nanosheets

$Co(NO_3)_2 \cdot nH_2O$ and $NiCl_2 \cdot 6H_2O$ from Sigma–Aldrich Co. LLC. are of analytical grade and used as starting materials without further purification. In a typical synthesis procedure, 1 mmol of $Co(NO_3)_2 \cdot nH_2O$ was dissolved in 20 mL deionized water, and then 1 mL of NH_4OH (28.0–30.0% NH_3 basis) was added dropwise under continuous stirring. The cluster formed and the mixture was transferred into a 45 mL vessel and sealed in a Parr 4848 autoclave. The autoclave was heated by a microwave oven (Panasonic, NN-SN778S, 2.45 GHz, maximum power 1250 W) with 40% of the maximum power of 1250 W for 3 min. After the reaction, the autoclave was cooled down to room temperature naturally. The resulting precipitate was collected and washed with absolute ethanol and de-ionized water in sequence for several times. The products were dried in a vacuum oven at 60 °C overnight. Subsequently, designed amount of $NiCl_2 \cdot 6H_2O$ was added and the concentration of metal ions was kept the same. The hybrid $Co_xNi_{1-x}(OH)_2$ nanosheets were prepared under the same condition.

2.2. Characterization

The phase and structure of the obtained products were determined on a Rigaku MiniFlex II X-ray powder diffractometer (XRD) with Cu Kα radiation (λ = 1.5418 Å). The operation voltage and current were kept at 40 kV and 30 mA, respectively. The size, morphology and lattice parameters were determined by Hitachi H-7650 transmission electron microscope (TEM), JEOL-2010 and FEI high resolution transmission electron microscope (HRTEM); Energy-dispersive X-ray spectroscopy (EDS) was taken on TEM.

2.3. Electrochemical test

The electrochemical performance was evaluated by galvanostatic charge/discharge cycling on LAND CT2001A multi-channel battery testing system at room temperature using a three electrode cell with 1 M KOH as the electrolyte, Ag/AgCl electrode as reference electrode, and platinum foil as counter electrode, respectively. For the preparation of the working electrode, 70 wt% of active materials, 20 wt% of carbon black, and 10 wt% of polyvinylidene fluorides (PVDF) were mixed in N-methyl-2-pyrrolidinone (NMP). The obtained slurry was cast onto nickel foam and dried in a vacuum oven at 80 °C for 12 h to remove the solvent. Specific capacitance could be calculated from the galvanostatic charge and discharge curves, using the following equation: $C = I\Delta t/m\Delta V$, where I is charge or discharge current, Δt is the time for a full charge or discharge, m indicates the mass of the active material, and ΔV represents the voltage window in a full charge–discharge process. The electrode loading amount is around 2.0 mg cm^{-2}. The cyclic voltammetry (CV) curves of as-prepared samples were obtained by a VersaSTAT 4 with a scan rate of 10 mV s^{-1}.

3. Results and discussion

Typical transmission electron microscopy (TEM) image shown in Fig. 1A indicates that well defined hexagonal nanosheets ($Co_{0.2}Ni_{0.8}(OH)_2$) can be successfully obtained on a large scale *via* the microwave-assisted route. As shown in Fig. 1B, the diameter of uniform hexagonal nanosheets can be determined to be 100–150 nm. The thickness of a single nanosheet can be calculated to be around 15.6 nm in Fig. 1C. Fig. 1D is a typical HRTEM image obtained on an individual $Co_{0.2}Ni_{0.8}(OH)_2$ nanosheet, indicating that the nanosheet is structurally uniform with an interlayer spacing of about 0.234 nm, which corresponds to the (101) lattice plane. The inset Fast Fourier Transform (FFT) image of select area also confirms the good crystallinity of the hexagonal nanosheet. It is noteworthy that the size of final hexagonal nanosheets decreases with the increase amount of nickel as shown in Figure S1A–D. The average diameters of $Co(OH)_2$ and $Co_{0.8}Ni_{0.2}(OH)_2$ nanosheets are about 1 μm and 400 nm, respectively. However, the average width of the nanosheets became comparable with each other with the amount of nickel above 20%, which was measured to be 200 and 160 nm for $Co_{0.5}Ni_{0.5}(OH)_2$ and $Ni(OH)_2$ nanosheets, respectively. It should be pointed out that there are small particles in the products when the amount of cobalt precursor is over 50%. For the pure $Co(OH)_2$, the particles in the products were also demonstrated to be single $Co(OH)_2$ crystal as shown in Figure S3. The HRTEM images of Co–Ni hydroxide nanosheet with different Co:Ni ratio were shown in Figure S1E–H. Interestingly, the interplanar spacing study demonstrates that the increase of cobalt in products will consecutively enlarge the *d*-spacing of (101) lattice plane, which is in good agreement with the X-ray diffraction (XRD) results.

XRD was also carried out to determine the structure and crystallinity of the as-prepared products. Fig. 2A shows typical XRD pattern of as-obtained products with different Co:Ni ratios. All diffraction peaks in the XRD pattern can be indexed as the hexagonal Co–Ni hydroxides (space group: *P3_m1* (No. 164)). No other peak was observed, indicating the high purity of Co–Ni hydroxide. Careful observation shows that the peaks shift a little bit to the high angle with the increase amount of nickel. The strongest diffraction peak which corresponds to the (101) lattice plane was chosen to

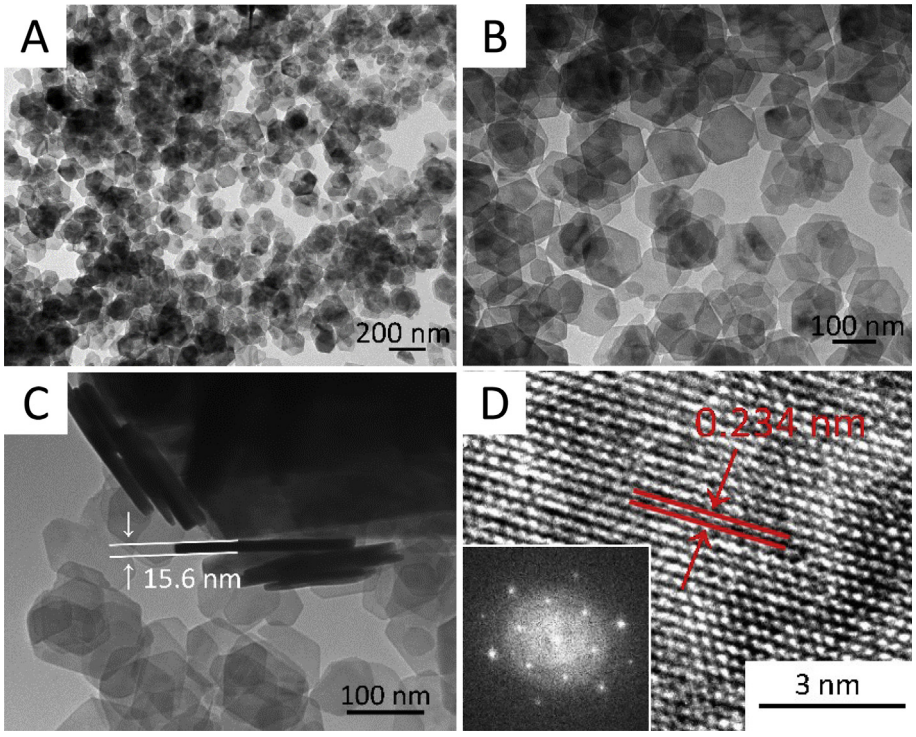

Fig. 1. Typical TEM images of as-prepared $Co_{0.2}Ni_{0.8}(OH)_2$ hexagonal nanosheets at (A) low; (B) middle; (C) high magnification; and (D) HRTEM image. Inset in (D) is FFT image of selected area.

calculate the *d*-spacing of (101). The calculated *d*-spacing of (101) from HRTEM and XRD is listed in Fig. 2B and Table S1. The both physical and chemical similarities of Co and Ni enable the structural compatibility. There is only slight differences between the samples with different ratios of Co:Ni. For the counterpart, the *d*-spacings of (101) lattice plane for both $Co(OH)_2$ and $Ni(OH)_2$ are close to the theoretical values in standard PDF files. The hybrid Co–Ni hydroxides display linearly increasing feature in *d*-spacings of (101) with the increase amount of cobalt, which could provide an evidence for the rational design of hybrid transition metal oxide or hydroxide materials.

The elemental maps of an individual $Co_{0.5}Ni_{0.5}(OH)_2$ nanosheet are displayed in Fig. 3, which clearly demonstrates a homogeneous distribution of Co, Ni, and O elements. The line-scan analysis in Figure S2 reveals the profile of Co and Ni atoms across the radial direction, indicating an apparent layered nature. Only Co, Ni, and O elements were detected and the molar ratio of Co:Ni:O is about 13.6:11.7:74.6 (or 1.16:1:6.4), which is slightly different from the theoretical element concentration ratio of 1:1:4 calculated from the chemical formula. It could be ascribed to the absorbed oxygen species on the surface of nanosheets. These results further confirm that Co and Ni were indeed incorporated into the host layer of hydroxide nanosheet without segregation.

The electrochemical properties of as-obtained $Co_xNi_{1-x}(OH)_2$ (x = 0, 0.2, 0.5, 0.8, 1.0) nanosheets were investigated by cyclic voltammetry (CV) and galvanic charge–discharge (CD) in a three-electrode cell with a Ag/AgCl reference electrode and 1 M KOH aqueous electrolyte. Fig. 4A shows typical CV curves at a scan rate of 10 mV s^{-1}. The high voltage edge was tuned a little bit to avoid the serious electrolysis reaction of H_2O. The redox current peaks could be explicitly observed, which can be attributed to a combined effect of the following redox reactions derived from transition-metal

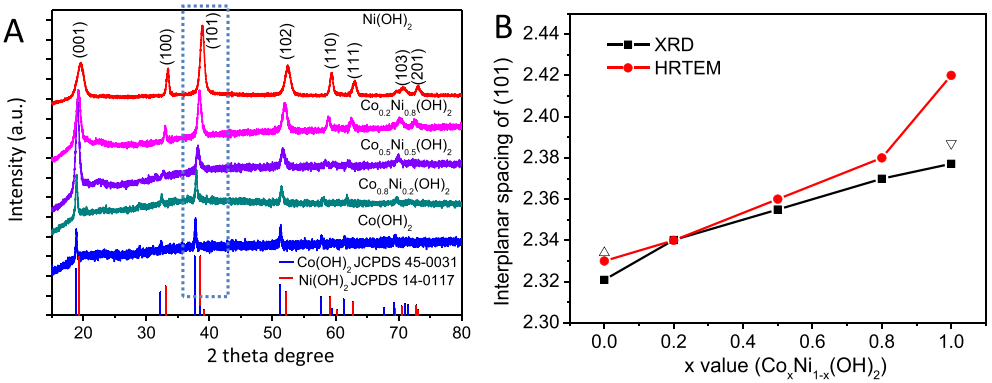

Fig. 2. (A) XRD pattern of $Co_xNi_{1-x}(OH)_2$ nanosheets; (B) *d*-spacing of (101) lattice plane indicated from XRD and HRTEM. △ and ▽ are theoretical *d*-spacing of $Ni(OH)_2$ (JCPDS 14-0117) and $Co(OH)_2$ (JCPDS 45-0031) calculated from standard PDF files, respectively.

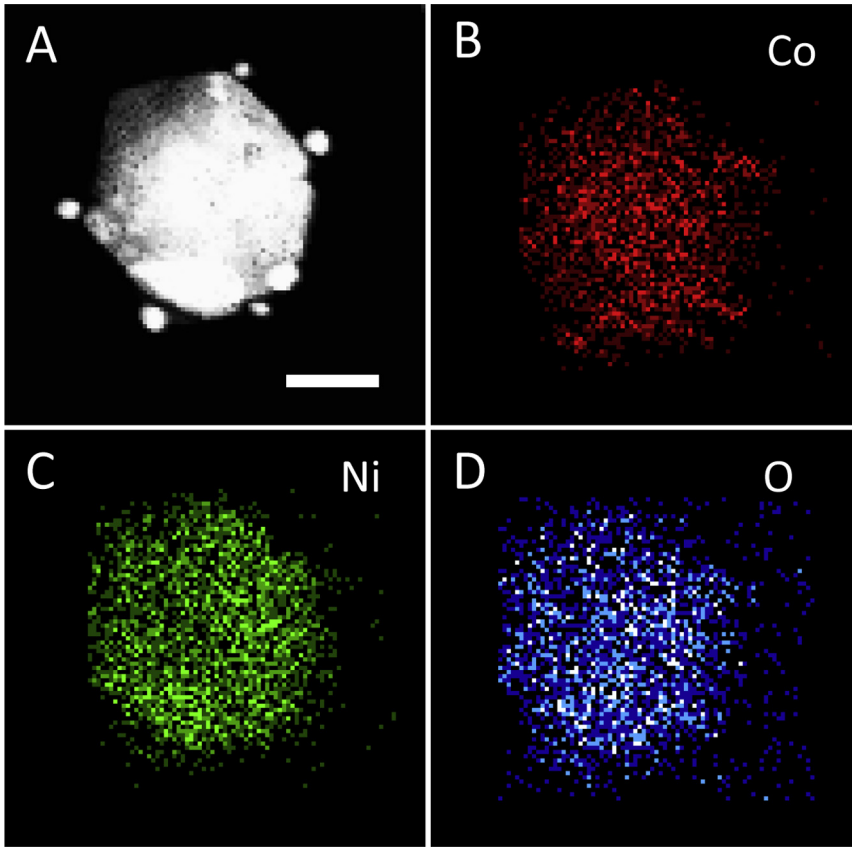

Fig. 3. (A) TEM image of an individual $Co_{0.5}Ni_{0.5}(OH)_2$ nanosheet and the scale bar is 50 nm; EDS elemental maps taken from the same area are (B) Co, (C) Ni, and (D) O, respectively.

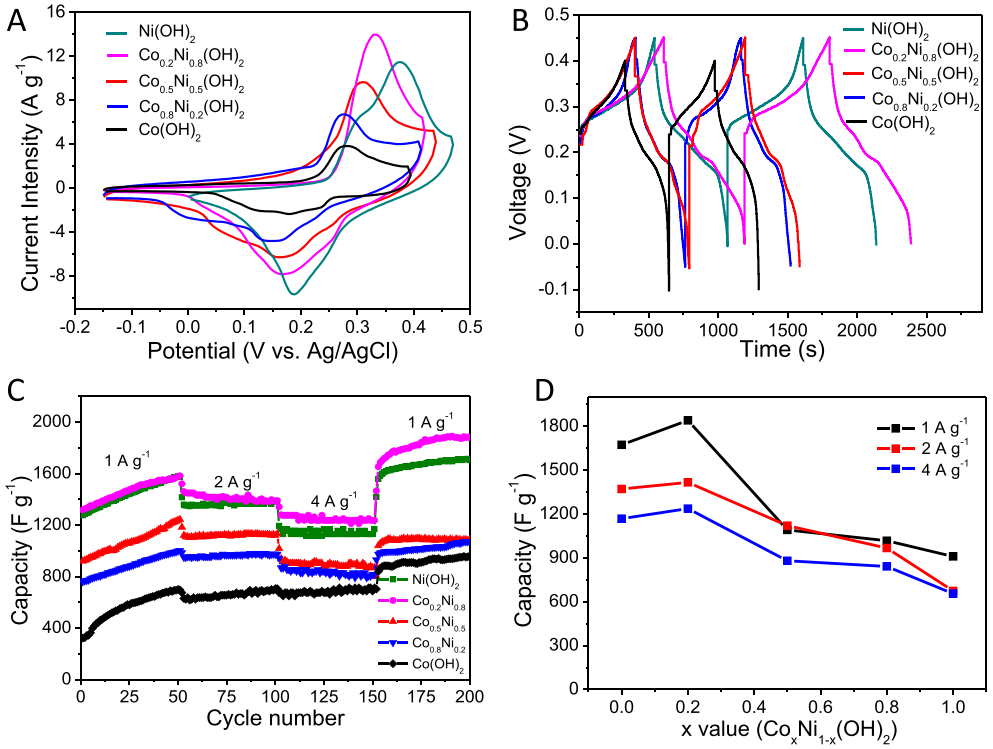

Fig. 4. Electrochemical performances of Co–Ni hydroxide nanosheets with different Co–Ni composition: (A) CV curves at a scan rate of 10 mV s^{-1}; (B) specific capacitance of nanosheets at a charge and discharge current density of 1 A g^{-1}; (C) rate performance at different current densities; (D) specific capacitance of the $Co_xNi_{1-x}(OH)_2$ nanosheets as a function of composition at different current densities.

hydroxides: $Co(OH)_2 + OH^- \leftrightarrow CoOOH + H_2O + e^-$ and $Ni(OH)_2 + OH^- \leftrightarrow NiOOH + H_2O + e^-$, respectively [29–33]. The anodic and cathodic sweeping indicates that the oxidation and the reduction peaks at 188 mV and 375 mV for monometallic $Ni(OH)_2$ nanosheets shift to 110 mV and 280 mV for monometallic $Co(OH)_2$ nanosheets, respectively, due to the lower redox potential of $Co(OH)_2$/CoOOH couple. For the CV profiles of $Co(OH)_2$ and $Co_{0.8}Ni_{0.2}(OH)_2$, not obvious anodic or cathodic shift was observed. On the other hand, it should be pointed out that the oxidation and the reduction peaks are gradually enhanced and shifted to a higher potential with the increase of Ni content in the bimetallic Co_xNi_{1-x} ($x = 0.8, 0.5, 0.2$) host slabs. The highest redox current was observed for $Co_{0.2}Ni_{0.8}(OH)_2$ nanosheets, indicating the feasibility of rationally tuning the Co:Ni ratio for optimizing electrochemical performance.

Fig. 4B shows the typical charge–discharge curves of $Co_xNi_{1-x}(OH)_2$ nanosheets at a galvanic current density of 1 A g^{-1}. The specific capacitances are approximate 909, 1017, 1091, 1840, and 1673 F g^{-1} for $Co(OH)_2$, $Co_{0.8}Ni_{0.2}(OH)_2$, $Co_{0.5}Ni_{0.5}(OH)_2$, $Co_{0.2}Ni_{0.8}(OH)_2$, and $Ni(OH)_2$ nanosheets, respectively. Interestingly, the specific capacitances of Co–Ni hydroxides nanosheets generally increase with the increase of nickel amount. The highest capacitance appears at the Co:Ni ratio of 0.2:0.8. Consistent with the CV profiles, $Co_{0.2}Ni_{0.8}(OH)_2$ nanosheets possess the highest specific capacitance, which may be attributed to the enhancement of the electro-active sites participated in the redox reaction due to possible valence interchange or charge hopping between Co and Ni cations [19,34]. On the other hand, the thin layered feature and large interlamellar spacing also provide more reaction sites and facilitate the ion transfer. Fig. 4C and D shows the rate performance of as-products at different current densities. Generally, the capacitance of the five samples is increasing when the initial current density was set as 1 A g^{-1} for the first 50 cycles. Then they platform when the current density was increased to 2 and 4 A g^{-1} in the following cycles. For the monometallic $Co(OH)_2$ nanosheets, the large size might be another factor for its low capacity. The hybrid $Co_{0.2}Ni_{0.8}(OH)_2$ hexagonal nanosheets deliver the highest capacity of 1240 F g^{-1} among the five at a current density of 4 A g^{-1}. No obvious decrease in capacity was observed for all of the samples. After the current density was reset to 1 A g^{-1}, the capacity can rebound to a higher level and become relatively stable with the increase of cycles. From Fig. 4D, it can be easily identified that the $Co_{0.2}Ni_{0.8}(OH)_2$ is an optimal composition with the best performance. Then the cycling performance of $Co_{0.2}Ni_{0.8}(OH)_2$ nanosheets was further investigated. As shown in Figure S4, the cycling response with a steplike profile at successive rates can be evidently observed. Together with the increase of discharging current rates, the average capacitance of $Co_{0.2}Ni_{0.8}(OH)_2$ nanosheets can be measured around 1400 F g^{-1} (at 2 A g^{-1}), 1170 F g^{-1} (4 A g^{-1}), and 988 F g^{-1} (8 A g^{-1}), respectively. The Coulombic efficiency could be maintained above 95% except for those at the current changing points and the retention of capacity in the cycling at each current density can be determined over 94%. Such high cycling capacity and high rate capability enable them to be potential active materials for supercapacitors in next-generation energy storage field. Taking advantage of their tunable compositions and thin sheet feature, the hybrid Co–Ni hydroxide nanosheets show promising applications for the development of high-performance energy storage devices and may provide certain clue for improving the electrochemical performance by a simple doping strategy.

4. Conclusion

In summary, a facile microwave-assisted strategy was successfully developed for the preparation of hybrid Co–Ni hydroxide nanosheets with controllable transition-metal composition. The lattice spacing of the Co–Ni hydroxide nanosheets can be slightly tuned by changing the metal ratio of Co:Ni in the final products. The electrochemical studies revealed that hybrid hydroxide nanosheets exhibit a high specific capacity and excellent cycling stability, and can be used as promising candidate for the application in a high-performance supercapacitor. The present facile microwave-assisted route for the synthesis of Co–Ni hydroxides is expected to be applied to other transition-metal hydroxides and oxides as well. Moreover, the optimization of electrochemical properties by changing the composition in the final products could be a very useful strategy in improving the electrochemical performances, which could provide further insights in the material design.

Acknowledgements

H.L. acknowledges the funding support from NSF/CMMI Nano-Manufacturing Program under Grant No. 1131290. G. C. is supported by the office of Vice President for Research at NMSU. S. S. L. is supported by NASA under Grant No. GR0003400. This work is partially supported by the U.S. Department of Energy, Office of Basic Energy Sciences, Division of Materials Sciences and Engineering. Sandia is a multiprogram laboratory operated by Sandia Corporation, a wholly owned subsidiary of Lockheed Martin Corporation, for the U.S. Department of Energy's National Nuclear Security Administration under Contract DE-AC04-94AL85000.

Appendix A. Supplementary material

Supplementary data related to this article can be found at http://dx.doi.org/10.1016/j.jpowsour.2013.11.070.

References

[1] S. Chu, A. Majumdar, Nature 488 (2012) 294–303.
[2] N.-S. Choi, Z. Chen, S.A. Freunberger, X. Ji, Y.-K. Sun, K. Amine, G. Yushin, L.F. Nazar, J. Cho, P.G. Bruce, Angew. Chem. Int. Ed. 51 (2012) 9994–10024.
[3] M.M. Thackeray, C. Wolverton, E.D. Isaacs, Energy Environ. Sci. 5 (2012) 7854–7863.
[4] G. Wang, L. Zhang, J. Zhang, Chem. Soc. Rev. 41 (2012) 797–828.
[5] K. Naoi, S. Ishimoto, J.-i. Miyamoto, W. Naoi, Energy Environ. Sci. 5 (2012) 9363–9373.
[6] M. Zhi, C. Xiang, J. Li, M. Li, N. Wu, Nanoscale 5 (2013) 72–88.
[7] Y.M. He, W.J. Chen, X.D. Li, Z.X. Zhang, J.C. Fu, C.H. Zhao, E.Q. Xie, ACS Nano 7 (2013) 174–182.
[8] Z.X. Song, W. Liu, M. Zhao, Y.J. Zhang, G.C. Liu, C. Yu, J.S. Qiu, J. Alloy Compd. 560 (2013) 151–155.
[9] K. Liang, X.Z. Tang, W.C. Hu, J. Mater. Chem. 22 (2012) 11062–11067.
[10] C.Z. Yuan, L. Yang, L.R. Hou, L.F. Shen, X.G. Zhang, X.W. Lou, Energy Environ. Sci. 5 (2012) 7883–7887.
[11] F. Zhang, C.Z. Yuan, X.J. Lu, L.J. Zhang, Q. Che, X.G. Zhang, J. Power Sources 203 (2012) 250–256.
[12] J.A. Jiang, J.P. Liu, R.M. Ding, J.H. Zhu, Y.Y. Li, A.Z. Hu, X. Li, X.T. Huang, ACS Appl. Mater. Interf. 3 (2011) 99–103.
[13] L. Wang, Z.H. Dong, Z.G. Wang, F.X. Zhang, J. Jin, Adv. Funct. Mater. 23 (2012) 2758–2764.
[14] J. Xie, X. Sun, N. Zhang, K. Xu, M. Zhou, Y. Xie, Nano Energy 2 (2013) 65–74.
[15] C. Yuan, J. Li, L. Hou, X. Zhang, L. Shen, X.W. Lou, Adv. Funct. Mater. 22 (2012) 4592–4597.
[16] G.Q. Zhang, X.W. Lou, Adv. Mater. 25 (2013) 976–979.
[17] H.B. Wu, H. Pang, X.W. Lou, Energy Environ. Sci. (2013), http://dx.doi.org/10.1039/C3EE42101E.
[18] L.J. Xie, Z.A. Hu, C.X. Lv, G.H. Sun, J.L. Wang, Y.Q. Li, H.W. He, J. Wang, K.X. Li, Electrochim. Acta 78 (2012) 205–211.
[19] V. Gupta, S. Gupta, N. Miura, J. Power Sources 175 (2008) 680–685.
[20] X. Liu, R. Ma, Y. Bando, T. Sasaki, Adv. Mater. 24 (2012) 2148–2153.
[21] M. Vidotti, R.P. Salvador, E.A. Ponzio, S.I. Cordoba de Torresi, J. Nanosci. Nanotechnol. 7 (2007) 3221–3226.
[22] L. Tian, K.L. Huang, Y.N. Liu, S.Q. Liu, J. Solid State Chem. 184 (2011) 2961–2965.
[23] Q.J. Chen, N. Wang, L. Guo, Res. Chem. Intermed. 37 (2011) 421–428.
[24] F. Cao, G.X. Pan, P.S. Tang, H.F. Chen, J. Power Sources 216 (2012) 395–399.
[25] C.Z. Yuan, L. Yang, L.R. Hou, D.K. Li, L.F. Shen, F. Zhang, X.G. Zhang, J. Solid State Electrochem. 16 (2012) 1519–1525.

[26] M. Baghbanzadeh, L. Carbone, P.D. Cozzoli, C.O. Kappe, Angew. Chem. Int. Ed. 50 (2011) 11312–11359.
[27] X. Liu, R. Ma, Y. Bando, T. Sasaki, Angew. Chem. Int. Ed. 49 (2010) 8253–8256.
[28] H.-Y. Hsu, K.-H. Chang, R.R. Salunkhe, C.-T. Hsu, C.-C. Hu, Electrochim. Acta 94 (2013) 104–112.
[29] J.W. Lee, J.M. Ko, J.-D. Kim, J. Phys. Chem. C 115 (2011) 19445–19454.
[30] S. Chen, J. Zhu, X. Wang, J. Phys. Chem. C 114 (2010) 11829–11834.
[31] T. Xue, X. Wang, J.M. Lee, J. Power Sources 201 (2012) 382–386.
[32] T. Wu, C.Z. Yuan, Mater. Lett. 85 (2012) 161–163.
[33] Z.-A. Hu, Y.-L. Xie, Y.-X. Wang, H.-Y. Wu, Y.-Y. Yang, Z.-Y. Zhang, Electrochim. Acta 54 (2009) 2737–2741.
[34] W. Chen, Y. Yang, H. Shao, J. Fan, J. Phys. Chem. C 112 (2008) 17471–17477.